RMetS
Royal Meteorological Society

Seasonal and interannual variability of an index of deep atmospheric convection over western boundary currents

L. Sheldon and A. Czaja*
Department of Physics, Imperial College, London

*Correspondence to: A. Czaja, Huxley Building, Room 726, Imperial college, Prince Consort Road, London, SW7 2AZ.
E-mail: l.sheldon11@imperial.ac.uk

The seasonal and interannual variability of an index measuring the potential for deep (surface-to-tropopause) convection over the extratropical oceans is studied using reanalysis data. It is found that most of the conditional instability is concentrated over the world's western boundary currents during winter, but shifts equatorward of the currents in summer. Conditional instability is only detected over the Gulf Stream and the East Australian Current in their respective summer season.

The coupled ocean–atmosphere mechanisms controlling the variability of the convective index are then studied. It is found that the convective index displays a large interannual variability, which is primarily controlled by the erratic displacements of the storm tracks. Only weak negative feedback from the oceans is singled out on short (intraseasonal) time-scales, reflecting the stabilization of the troposphere through the development of cold sea-surface temperature anomalies. A larger role for warm oceanic advection in destabilizing the troposphere is, however, suggested on longer (interannual and decadal) time-scales. Copyright © 2013 Royal Meteorological Society

Key Words: convection; air–sea interaction; midlatitude climate variability

Received 1 June 2012; Revised 9 November 2012; Accepted 7 December 2012; Published online in Wiley Online Library

Citation: L. Sheldon, A. Czaja. 2013. Seasonal and interannual variability of an index of deep atmospheric convection over western boundary currents. *Q. J. R. Meteorol. Soc.* DOI:10.1002/qj.2103

1. Introduction

There has recently been a resurgence of studies dedicated to ocean–atmosphere coupling in midlatitudes, which suggests that coarse climate models might not capture some of the oceanic impact on the atmosphere inferred from observations. Indeed, although general circulation models find the internal variability of the atmosphere to be far greater than the influence of ocean forcing (Kushnir *et al.*, 2002), recent observational studies indicate that the ocean forcing could be greater than previously expected and the underlying processes may not be resolved or represented in the models. For example, high-resolution satellite observations have suggested that fronts in sea-surface temperature (hereafter SST) influence both the curl and divergence of wind fields (Chelton *et al.*, 2004; Small *et al.*, 2008). This influence has been shown to reach above the marine–atmosphere boundary layer in one or more indicators in the form of of clouds, lightning, vertical velocities and precipitation for the Agulhas Current (Liu *et al.*, 2007), the Kuroshio Extension (Tokinaga *et al.*, 2009) and the Gulf Stream (Minobe *et al.*, 2008; Zhai and Sheldon, 2012). Reanalysis data have also consistently provided support for an impact of SST anomalies on the atmospheric circulation in the North Atlantic (Czaja and Frankignoul, 2002) and the North Pacific (Frankignoul *et al.*, 2011).

In a recent study, Czaja and Blunt (2011, hereafter CB) suggested that moist convection occurring in the frontal systems embedded in extratropical cyclones could be an important mechanism 'transferring' changes in SST upwards into deep layers of the atmosphere. CB introduced a simple index of the degree of instability of the atmosphere to moist

convection and showed that in winter it peaks over all western boundary-current systems of the world's oceans, with the exception of the Brazil–Malvinas confluence region. It is the purpose of this study (i) to extend the initial findings of CB (they only discussed one winter season) by analyzing the seasonal and interannual variability of the convective index in a 32 yr long dataset and (ii) to investigate the mechanisms controlling the degree of convective instability of the ocean–atmosphere system over western boundary currents.

The article is structured as follows. In section 2, the convective index and the data used are briefly introduced. The seasonal and interannual variability of the convective index are described in sections 3 and 4, respectively. Coupled ocean–atmosphere feedback is investigated in section 5. A conclusion is offered in section 6.

2. An index of deep convection over the oceans

An air parcel displaced vertically in a saturated environment will not return to its initial position if the moist entropy of the environment decreases with height* (Emanuel, 1994). Accordingly, a simple measure of convective instability for a deep layer of saturated air extending from the sea surface (at specific entropy s_{surf}) to the tropopause (at specific entropy s_{tp}) is that $s_{tp} - s_{surf} < 0$. In practice, were such a deep unstable layer found, it would quickly overturn and adjust to a state of neutrality to moist convection ($s_{tp} = s_{surf}$). As a result, it is more physically relevant to look for a necessary condition for instability by investigating situations in which the entropy of the low-level air is set to an upper limit s_o while still satisfying the inequality

$$s_{tp} - s_o < 0. \tag{1}$$

Considering that it is only far removed from continental boundaries that a low-level air parcel is thermodynamically adjusted with the ocean, a plausible choice for s_o is the specific entropy that an air parcel would have at a relative humidity of 80% (the typical relative humidity in the marine boundary layer in the open ocean) and at the same temperature as the sea surface. Criterion (1) with this definition of s_o thus provides an upper bound on the occurrence of convective instability from the sea surface to the tropopause and this was the basis for the index studies in CB.

We examine below the number of days within a given season where (1) is met in the ERA interim dataset (Berrisford *et al.*, 2009) provided on a $0.7^\circ \times 0.7^\circ$ horizontal grid over a 32 yr period (1979–2011) at 1200 UTC each day. Following the methodology in CB, the specific entropy (s) is calculated according to Emanuel (1994):

$$\begin{aligned} s =& [q_T c_l + (1 - q_T)\, c_{pd}] \ln \frac{T}{T_o} \\ & - R_d (1 - q_T) \ln \frac{(P - e)}{P_o} \\ & + \frac{l_v q_v}{T} - R_v q_v \ln RH, \end{aligned} \tag{2}$$

in which the temperature (T), specific humidity (q_v), water-vapour presssure (e), total pressure (P), total water content (q_T) and relative humidity (RH) were taken from the daily (1200 UTC) fields of ERA-interim data. In (2), $T_o = 273.15$ K is a reference temperature and $P_o = 1000$ mb a reference pressure, while c_l is the specific heat capacity of liquid water, c_{pd} that of dry air at constant pressure, R_d and R_v the gas constants for dry air and vapour respectively and l_v the enthalpy of vaporization.

At a given time, the tropopause is tracked by following the surface of 2 PV units (after Hoskins *et al.*, 1985). In practice, moisture levels are so low at this level that (2) reduces approximately to the specific entropy of dry air at the tropopause temperature (T_{tp}) and pressure (P_{tp}):

$$s_{tp} \approx c_{pd} \ln \frac{T_{tp}}{T_o} - R_d \ln \frac{P_{tp}}{P_o}. \tag{3}$$

The tropopause's entropy decreases when T_{tp} decreases or when the tropopause is depressed (higher P_{tp}). In practice, the temperature and pressure effects tend to cancel since when the tropopause moves closer to the Earth's surface both the pressure and temperature increase. Inspection of scatter plots of s_{tp} versus T_{tp} and P_{tp} reveals that pressure effects dominate (not shown). This is consistent with the idea that a low tropopause 'sucks in' potential temperature surfaces from below (Hoskins *et al.*, 1985). In simple terms, this means that low tropopause events are those we are particularly interested in since they will favour the satisfaction of criterion (1). Note that although (3) is simpler, s_{tp} was computed using the full expression (2) by interpolating all required variables (e.g. relative humidity in addition to P_{tp} and T_{tp}) on the 2 PV unit surface.

The calculation of s_o is as stated above, i.e. by using (2) with T = SST, $RH = 80\%$ and P set to the observed surface pressure (hereafter SP).

The convective index used here is not a standard metric of convection and one might rightly wonder whether it actually relates to convective instability throughout the air column. To address this question, in Figure 1 we compare the skill of our index in relating to convective precipitation with the skill obtained when using instead the convective available potential energy (CAPE), a more widely used measure of convective instability. Both CAPE and convective precipitation were obtained from the daily ERA-interim forecast dataset at 1200 UTC. The median CAPE value for each 4 percentile bin of convective precipitation in the Gulf Stream region (35–45°N, 40–80°W) during 10 winters (2001–2010) is plotted in Figure 1(a). This shows that CAPE is strongly related to convection, as the median value increases monotonically with convective precipitation. The calculation based on our convective index is shown in Figure 1(b), which displays the percentage of events for each 4 percentile bin of convective precipitation that satisfies condition (1) (grey line). As was found with CAPE, (1) is satisfied increasingly at higher convective precipitation, which supports our interpretation of the $s_{tp} - s_o$ index as an alternative measure of convection. Indeed, the main difference between Figure 1(b) and 1(a) is the linear dependence upon convective precipitation found with our index as opposed to the more complex exponential dependence found with CAPE. The main reason why we focus on the $s_{tp} - s_o < 0$ index rather than CAPE in this study is that, besides being simpler to compute than CAPE, our convective index explicitly uses SST, which allows a more straightforward analysis of ocean–atmosphere feedback than when using CAPE. We build on this strength in section 5 below.

*Small terms depending on the total water content need to be neglected in Emanuel's equation (6.2.10) for this statement to be true.

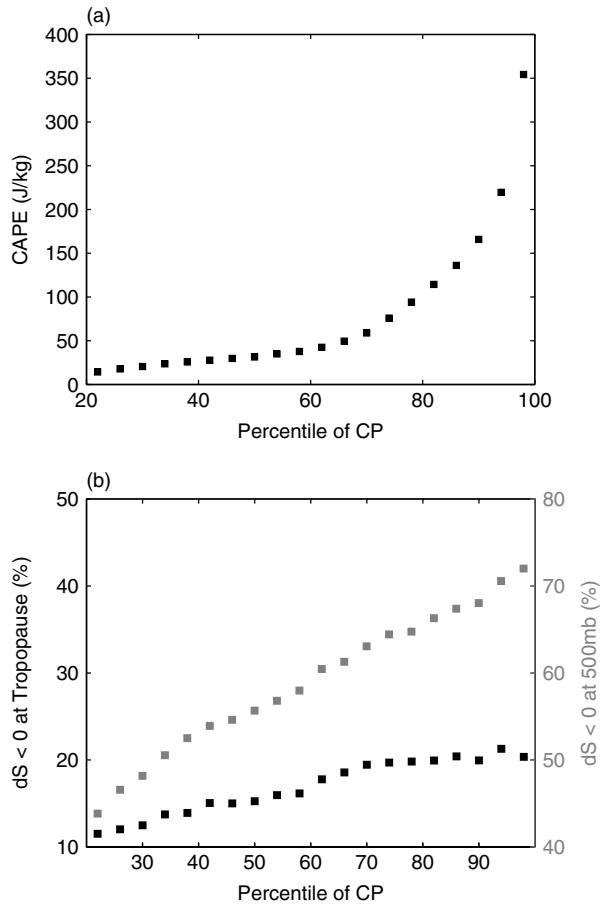

Figure 1. (a) The median CAPE for each percentile of convective precipitation (CP) over the Gulf Stream winter. (b) The percentage of events for each 4 percentile bin of convective precipitation over the Gulf Stream winter that satisfy the criteria $s_{tp} - s_o < 0$ (black) and $s_{500mb} - s_o < 0$ (grey). Both panels are for winters 2001–2010.

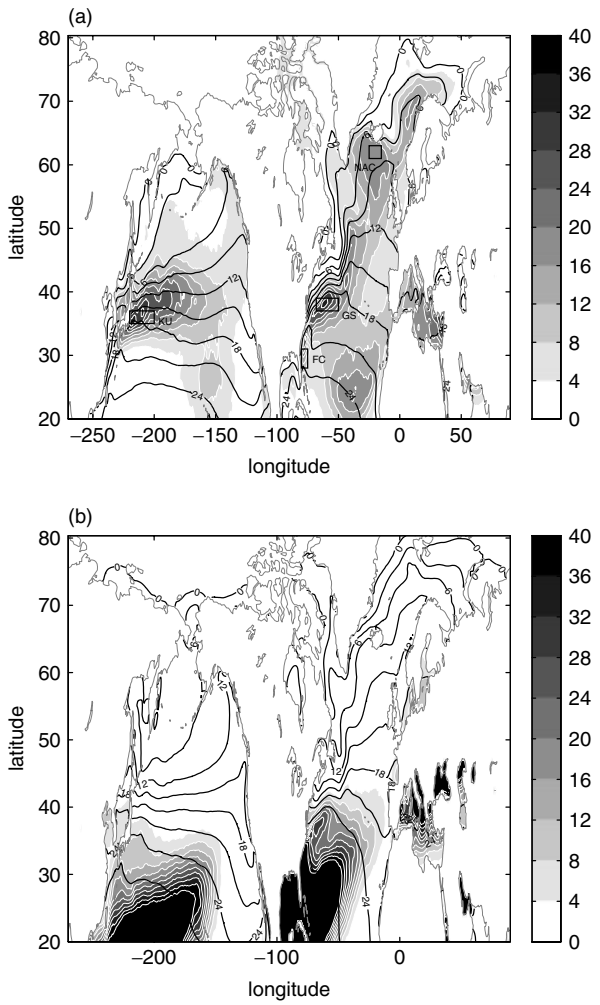

Figure 2. The filled contours show the mean fraction of days (in %) for which criterion (1) is met in (a) winter (DJF) and (b) summer (JJA). The seasonal mean SST is contoured every 3 K in black contours. The boxes in (a) define the regions used in Figure 4.

The result in Figure 1(b) indicates that only 10–20% (left vertical axis) of the population of events with significant precipitation occurs when the condition $s_{tp} - s_o < 0$ is satisfied. This suggests that more often than not convection only reaches to a level located below the tropopause. This interpretation is confirmed by repeating Figure 1(b) but replacing s_{tp} by the entropy s_{500} of moist air at 500 mb (grey points): as can be seen on the right vertical axis, typically 60% of the population of events with significant precipitation occurs when the condition $s_{500} - s_o < 0$ is satisfied. We focus in the following on the rarer convective events that extend from the sea surface to the tropopause, which we refer to in the following as 'deep convective' events.

3. Seasonal variability of the convective index

The fraction of days for which condition (1) was met was computed for each of the 32 winters (December–February (DJF) in the Northern Hemisphere and June–August (JJA) in the Southern Hemisphere) and summers. The resulting averaged maps for the Northern Hemisphere are given in Figure 2. In winter (Figure 2(a)) the results from CB are recovered, with the Gulf Stream and Kuroshio appearing as the regions in which (1) is met most frequently (about 30% of the time). Occurrences of unstable situations are otherwise low over the extratropical oceans (10% or less). This finding contrasts sharply with the summertime map (Figure 2(b)), which shows that the atmosphere is most often unstable to upright displacements of low-level air parcels in broad regions found equatorward of the western boundary currents and with larger occurrences (in excess of 50%) than found over the Gulf Stream or Kuroshio in winter. These regions reflect the subtropical extension of the convective warm pools of the western North Atlantic and North Pacific. Interestingly, north of these regions it is only over the Gulf Stream that significant occurrences are found in summer. Over the Kuroshio, the signal seen in winter in Figure 2(a) does not appear in Figure 2(b).

The results for the Southern Hemisphere (Figure 3) follow a similar trend. In winter (Figure 3(a)), occurrences are low in most places except over the East Australian Current (40%) and Aghulas Current (20%). As found in CB, but now established more firmly by the use of a 32 yr record, the Brazil–Malvinas confluence region does not show up in this diagnostic. In summer (Figure 3(b)), the largest occurrences are found to be associated with the subtropical extension of the South Pacific Convergence Zone and, at higher latitudes, it is only over the East Australian Current that (1) is met frequently (of the order of 20% of the time).

The previous results suggest that western boundary currents globally have varying success in favouring unstable conditions for atmospheric convection in winter and

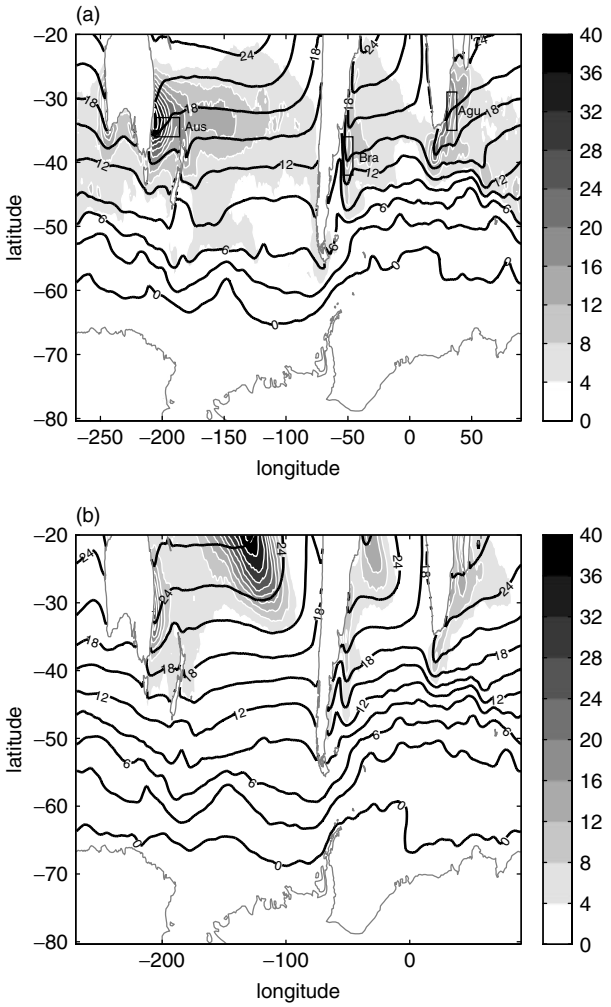

Figure 3. Same as Figure 1 but for the Southern Hemisphere (a) winter (JJA) and (b) summer (DJF).

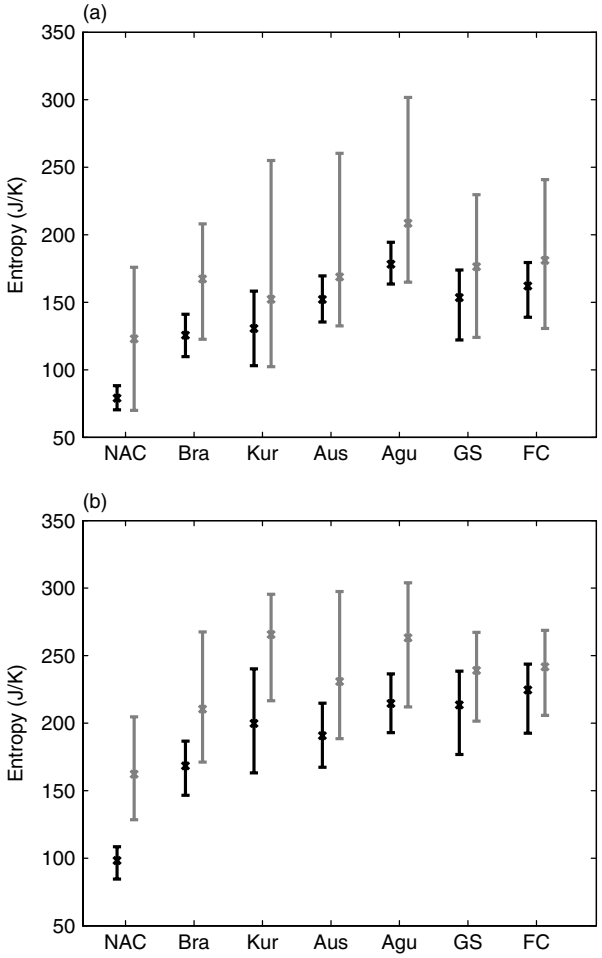

Figure 4. The median (diamonds), 10th (lower bar) and 90th (upper bar) decile of S_o (black) and S_{tp} (grey), in J K^{-1}, for the North Atlantic Current (NAC), Kuroshio (Kur), Australian Current (Aus), Agulhas Current (Aug), Brazil–Malvinas Current (Bra), Gulf Stream (GS) and Florida Current (FC). Panel (a) is for the current's winter and (b) is for the current's summer.

summer. Indeed, criterion (1) does not depend solely upon SST (and hence warm advection by the currents) but also upon atmospheric conditions (via s_{tp}). To analyze these two effects, the distribution of the 10th, 50th and 90th percentiles of s_o and s_{tp} for each western boundary current is shown in Figure 4. In winter (Figure 4(a)), the Brazil–Malvinas Current has one of the lowest surface entropies (black bars) of all currents (except for the North Atlantic Current), which is due to the lower SST along the Brazil–Malvinas Current compared with other currents (the regions covered in Figure 4 can be seen as the boxes in Figure 2 and 3). Since the tropopause entropy (grey bars) shows a similar distribution over the Brazil–Malvinas and East Australian Current, it can be safely concluded that this low SST is the reason why occurrences in Figure 3 are so low in the South Atlantic. When the SST is increased homogeneously by 2 K across the basin (not shown), the average occurrence of criterion (1) over the Agulhas Current in winter increases to over 20%.

The reason why the Gulf Stream was associated with significant occurrences in Figure 2 in summer, while the Kuroshio was not, can also be understood from Figure 4(b). It is seen that indeed the distributions of s_o and s_{tp} overlap significantly over the Gulf Stream but, in comparison, s_o is lower and s_{tp} higher over the Kuroshio. The different seasonality of occurrences over these two currents seen in Figure 2 thus reflects not only the lower SST of the Kuroshio but also the pattern of atmospheric stationary waves, which sets a different tropopause height over the North Atlantic and North Pacific.

Finally, an intriguing feature of Figure 2(a) is the presence of a significant number of days in winter where the convective criterion is met at high latitudes in the North Atlantic (typically 20% of the time). The seasonal mean SST contours (black in Figures 2 and 3) clearly relate this feature to the tongue of high temperature associated with the Gulf Stream's extension to the subpolar gyre. Nevertheless, it is seen in Figure 4(a) that, despite this warm advection, s_o in this region is the lowest of all surface entropies considered. It is only because the tropopause's entropy is low and extremely variable over high latitudes in the North Atlantic, which in effect is equivalent to saying that the tropopause pressure is low and extremely variable there, that criterion (1) can be met.

4. Interannual variability of the convective index

Maps of the standard deviation of the convective index for winter and summer are shown in Figure 5(a) and 5(b) respectively for the Northern Hemisphere and in Figure 6(a) and 6(b) for the Southern Hemisphere. It is seen that for all maps the largest standard deviations (in percentage of days

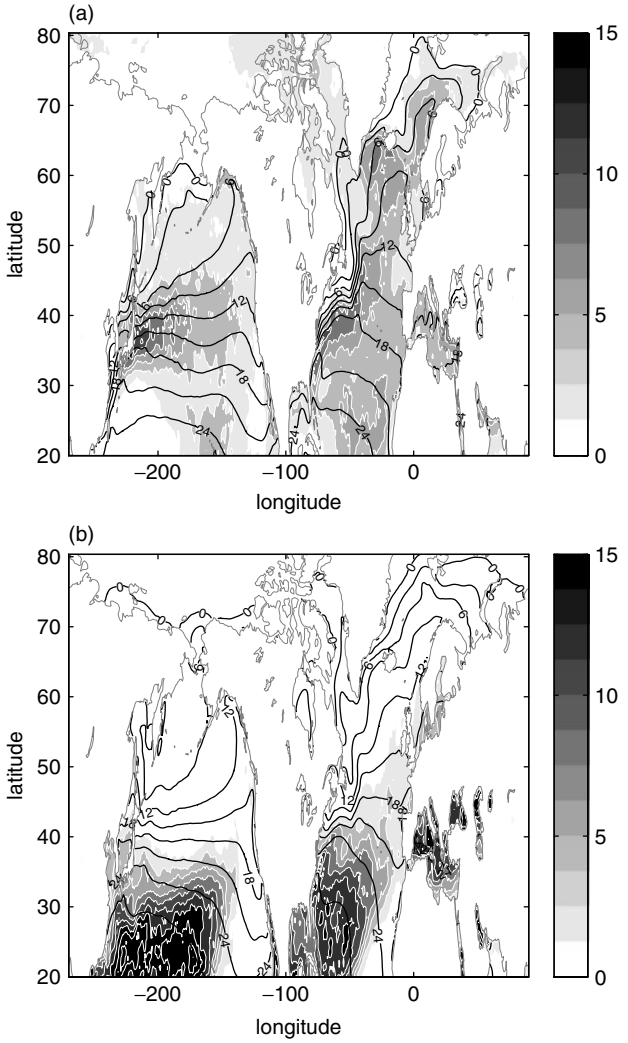

Figure 5. The standard deviation (filled contours) of the fraction of days (in %) for which criterion (1) is met in (a) winter (DJF) and (b) summer (JJA) for the Northern Hemisphere. The seasonal mean SST is contoured every 3 K in black contours.

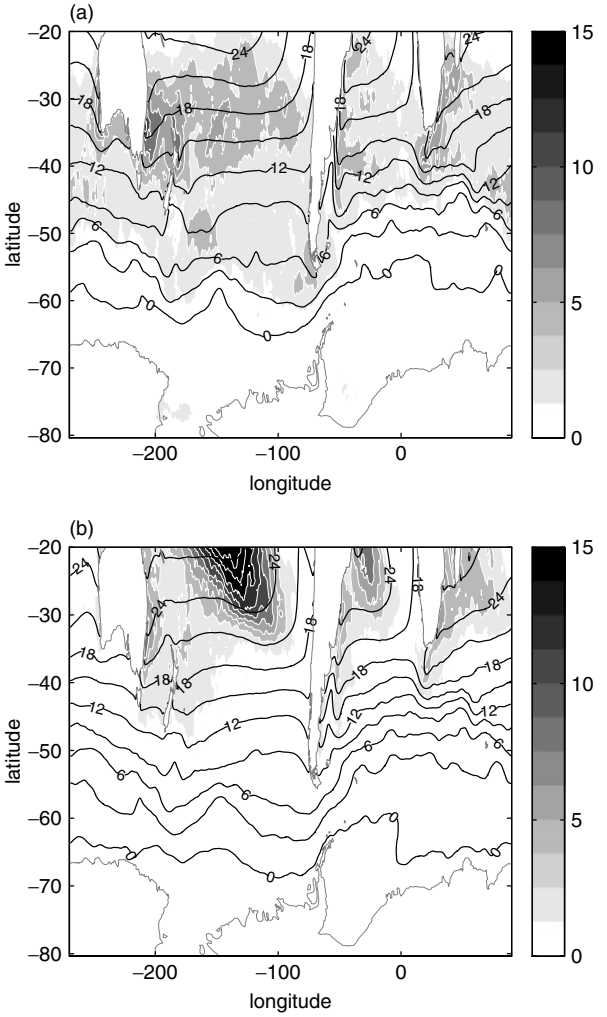

Figure 6. Same as Figure 5 but for the Southern Hemisphere in (a) winter (JJA) and (b) summer (DJF).

per season) coincide with the regions where, in the mean (Figures 2 and 3), criterion (1) is satisfied most frequently. The magnitude of the year-to-year variability is significant. In summer, peaks in Figures 2(b) and 3(b) occurred of the order of 50% of the time with, as seen in Figure 5(b), year-to-year fluctuations of the order of 15% of the time, i.e. a 30% relative change. Likewise, in winter the strong signals over the western boundary currents, which occurred of the order of 30% of the time in Figures 2(a) and 3(a), are seen in Figures 5(a) and 6(a) to be associated with year-to-year changes of the order of 10% of the time, again a relative change of 30%.

To help understand what controls the year-to-year fluctuations in atmospheric instability, we have performed an empirical orthogonal function (EOF) analysis of the 32 occurrence maps for a given season. Here, we solely discuss the results obtained in winter, since it is at that time of year that the western boundary currents systematically dominate the maps of occurrence of criterion (1) and, in addition, because the more tropical dynamics dominating the summer maps in Figures 2(b) and 3(b) might not be captured adequately by our choice of midlatitude-tied tropopause tracking (following a PV surface, as discussed in section 2). Table 1 summarizes the main statistics, with the regions used displayed in Figures 7 and 8. Note that removing a linear trend did not alter the results discussed below significantly, so we only show the analysis based on non-detrended data.

The dominant EOFs found in the North Atlantic and Pacific are shown in Figure 7(a) and 7(b), respectively. It is seen that, for both, the patterns are dipolar and account for fluctuations of the order of a few days per winter, although the magnitudes of both poles are not equal, with large asymmetry particularly in the North Pacific. The simple interpretation of the Northern Hemisphere EOF maps is that, for the phase indicated in the figure, when instability occurs more frequently over the western boundary currents (Kuroshio and Gulf Stream) it occurs less frequently further north and east. Conversely, in the opposite phase winters where instability occurs less frequently over the Gulf Stream are associated with more instability further north and east. In the North Atlantic, the associated time series correlates strongly (0.84) with the North Atlantic Oscillation (NAO) index, while in the North Pacific a similar level of correlation is found with the Western Pacific (WP) index.[†] The second EOFs (see Table 1) also correlate significantly in both basins

[†]All climate indices discussed here were downloaded from the National Weather Service Climate Prediction Centre, the Earth System research Laboratory or the British Antarctic Survey.

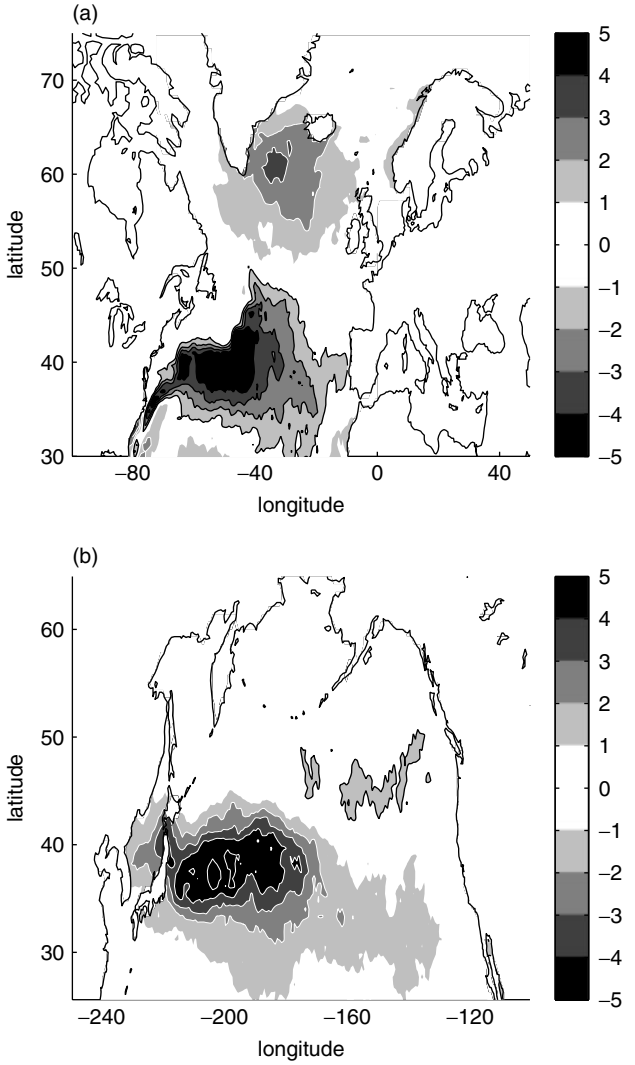

Figure 7. The first EOF of the winter mean fraction of days when criterion (1) occurs in (a) the North Atlantic (with intracontinental seas and basins masked) and (b) the North Pacific. Black contours are for positive values and white contours for negative values.

with a main mode of atmospheric variability (shown by correlation with the EOFs of the geopotential height at 500 mb or $Z500$) and, in the case of the Pacific, with the Pacific North American (PNA) pattern. These results support the view that the year-to-year variability in the number of days when (1) is met is primarily driven by the location of atmospheric storms, which set the regions where the tropopause entropy is low and variable. Indeed, the WP and NAO patterns share similar deflections of the storm tracks over their respective ocean basins (Linkin and Nigam, 2008).

The results for the Southern Hemisphere winter are shown in Figure 8(a) (South Pacific) and 8(b) (South Indian Ocean). As in the Northern Hemisphere, the first EOF is dipolar over the Agulhas Current, reflecting meridional shifts in instability over the Southern Indian Ocean. Over the East Australian Current, however (Figure 8(a)), the pattern is monopolar, indicating a modulation rather than a shift in the frequency of instability over the western boundary current. The main difference between the two hemispheres is the less clear link to modes of climate variability obtained in the Southern Hemisphere. Correlations of the time series associated with the EOF1 in Figure 8(a) and 8(b) with the Southern Annular Mode (SAM) or the Southern Oscillation Index (SOI) are not significant. However, as indicated in Table 1, significant correlations are found with the local EOF of 500 mb geopotential height (i.e. computed over the same domain as the EOFs in Figure 8(a) and 8(b)), supporting the idea that variations in the convective index over the Agulhas and East Australian Currents reflect more regional modes of atmospheric variability.

As a further test, we have repeated all the above EOF analyses by replacing the observed SST with a seasonally varying climatology. Consistent with the view that atmospheric variability is the main driver of year-to-year changes in the convective index by setting where and when the tropopause undulates most, we found virtually no change in the EOF patterns, fraction of variance explained, etc., when using climatological SSTs (not shown). The role of the ocean in contributing to the variability of the convective index is discussed further below.

Table 1. Correlations of the first three EOFs of the percentage of winter days when criterion (1) is met with the first two EOFs of the 500 mbar height ($Z500$) and the atmospheric modes (North Atlantic Oscillation (NAO), Pacific/North American pattern (PNA), Western Pattern (WP), Southern Annular Mode (SAM) and Southern Oscillation Index (SOI)) that directly affect the basin being considered. All numbers in bold have been deemed significant to 99% confidence level by performing permutation tests (this involves randomizing one of the two series 10 000 times and using the 99th percentile as a level of significance).

North Atlantic Basin					
		Correlation of principal component (PC) with:			
EOF	Variance (%)	$Z500$ PC (% variance)		Atmospheric Mode Index	
		1 (36%)	2 (18%)	NAO	
1	28%	**0.83**	0.15	**−0.82**	
2	19%	0.23	**0.76**	0.24	
3	10%	−0.03	−0.32	0.18	
North Pacific Basin					
		Correlation of principal component (PC) with:			
EOF	Variance (%)	$Z500$ PC (% variance)		Atmospheric Mode Index	
		1 (45%)	2 (20%)	PNA	WP
1	24%	−0.18	**−0.68**	0.15	**0.72**
2	17%	**0.80**	−0.21	**−0.75**	0.18
3	8%	−0.15	0.20	−0.01	−0.12
South Pacific Basin					
		Correlation of principal component (PC) with:			
EOF	Variance (%)	$Z500$ PC (% variance)		Atmospheric Mode Index	
		1 (30%)	2 (16%)	SAM	SOI
1	13%	**−0.66**	0.04	−0.29	0.28
2	10%	−0.11	−0.38	0.08	0.35
3	9%	0.11	−0.09	0.23	−0.29
South Indian Basin					
		Correlation of principal component (PC) with:			
EOF	Variance (%)	$Z500$ PC (% variance)		Atmospheric Mode Index	
		1 (44%)	2 (24%)	SAM	SOI
1	24%	0.21	**−0.46**	−0.20	0.31
2	18%	−0.18	−0.26	−0.02	0.01
3	6%	−0.15	0.09	−0.08	0.37

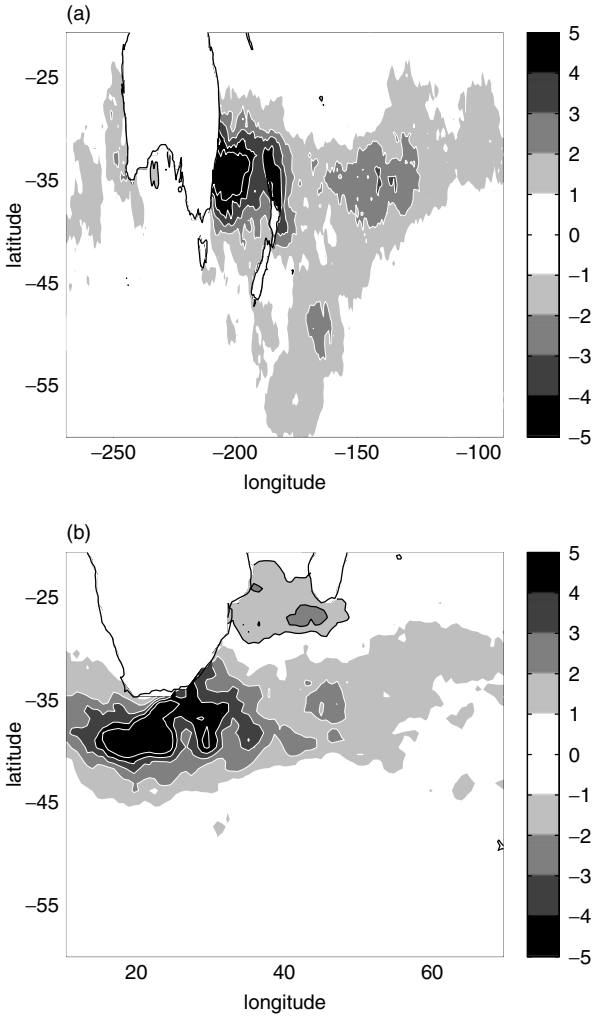

Figure 8. Same as Figure 6 but for (a) the South Pacific over East Australia and (b) the Indian Ocean around the Agulhas Current.

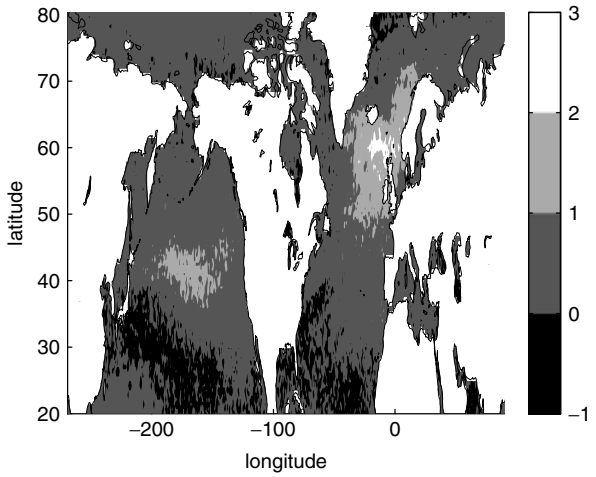

Figure 9. The difference (in days per winter) between the occurrence map in Figure 1(a) and that computed with wintertime mean SST and SSP. Positive values indicate a greater occurrence of convection in the interactive system. See text for details.

5. Coupled ocean–atmosphere feedback

To analyze the impact of changes in SST on the convective index it is convenient to distinguish between intraseasonal time-scales, over which SST anomalies likely reflect atmospheric forcing (surface heat fluxes, Ekman advection), and time-scales of years to decades, over which geostrophic ocean advection plays a more significant role (Frankignoul, 1985). As in the EOF analysis above we focus on wintertime.

5.1. Intraseasonal time-scales

When more low tropopause events occur than on average over a given region and season, this region becomes more likely to convect, since its average vertical stratification decreases. However, since low tropopause events usually couple with a developing low-pressure wave at low levels and an associated strengthening of the surface winds (Hoskins *et al.*, 1985), the resulting cooling of the upper ocean is expected to limit this 'preconditioning'.

To test whether the interaction of a synoptic system with the ocean indeed leads to negative feedback on this system on intraseasonal time-scales, we compare the frequency of occurrence of criterion (1), as shown in Figures 2 and 3, with the frequency of occurrence obtained with the same time history of s_{tp} but with intraseasonal anomalies in surface conditions (temperature and pressure) suppressed. To achieve this filtering, we recompute the surface entropy using, for a given winter, not the actual daily surface temperature and pressure but the linear trend of the latter estimated over that particular season[‡] (intraseasonal anomalies were also obtained by removing the smoothed seasonal cycle, which produced similar results, not shown).

The difference between the occurrence map in Figure 2 and the new one is shown in Figure 9 for the Northern Hemisphere (very similar results are found for the Southern Hemisphere, not shown). Typical differences are of the order of a few days at most, suggesting that the interaction with the upper ocean introduces a modulation of the convective index of the order of 10%. As expected from the above discussion, the difference map is negative over western boundary currents (dark shading), indicating less occurrence of convective instability in the interactive calculation than in the non-interactive one. However, there are also regions, typically at higher latitudes, where the difference map is positive (light shading). In these regions, intraseasonal anomalies in surface temperature and pressure thus lead to more occurrence of convective instability.

To understand this somewhat surprising result, we have computed the distribution of intraseasonal anomalies in SST and surface pressure found when the two calculations differ in sign (Table 2). Over the western boundary currents (upper two rows), it is seen that about $\approx$ 80% of the negative events seen in Figure 9 arise from negative SST anomalies of $\approx$ 0.3 K amplitude, as suggested above, and even more frequently ($\geqslant$ 90%) from positive SP anomalies of $\approx$ 6 mb amplitude. The latter is expected from the baroclinic nature of the storms over the western boundary currents, with a low tropopause above a high SP (see for example the schematic in CB11's figure 1). Both effects contribute equally to decreasing s_o and thus explain the reduction seen in Figure 9 over the western boundary currents. At higher latitudes (Table 2, bottom two rows) there is no association with SST anomalies of a particular sign but there is an overwhelming presence ($>$ 98%) of negative surface pressure anomalies of large amplitude ($\approx$ 20 mb). The negative SP anomalies

[‡]Note that in doing so the winter-to-winter fluctuations in s_o are kept.

Table 2. The intraseasonal anomalies of SST and SP for events when criterion (1) occurs in the full calculation (F_{full}) but does not in the calculation with intraseasonal anomalies in SST and SP removed (F_{filt}). The anomalies are split into positive and negative anomalies with their percentage of the total number of events also recorded. $F_{full} > F_{filt}$ indicates a greater occurrence of convection in the full calculation than in the one with intraseasonal anomalies in SST and SP removed.

Region	Event Criteria	SST anomaly					SP anomaly				
		Mean (K)	Positive %	Positive Value (K)	Negative %	Negative Value (K)	Mean (mbar)	Positive %	Positive Value (mbar)	Negative %	Negative Value (mbar)
Subtropical North Pacific	$F_{filt} < F_{full}$	−0.27	23%	0.19	**77%**	**−0.41**	6.4	**92%**	**7.1**	8%	−2.1
Subtropical North Pacific	$F_{filt} < F_{full}$	−0.20	21%	0.14	**80%**	**−0.29**	5.6	**94%**	**6.0**	6%	−2.2
Subpolar North Pacific	$F_{filt} > F_{full}$	0.04	51%	0.29	49%	−0.21	−18.0	1.3%	2.0	**98.7%**	**−18.2**
Subpolar North Atlantic	$F_{filt} > F_{full}$	0.04	55%	0.18	45%	−0.14	−22.9	0.3%	1.8	**99.7%**	**−23.0**

likely reflect the barotropic nature of the storms at the end of the storm track (Simmons and Hoskins, 1980), with a low tropopause associated with a low SP directly below it. The positive regions in Figure 9 are thus explained mostly by an atmospheric effect, the lowering of s_o associated with low SP.

5.2. *Interannual and longer time-scales*

A given season is a short time period in which to establish significant SST anomalies through surface cooling, and this must be the principal reason for the weakness of the negative feedback isolated above. On time-scales of years to decades much larger SST anomalies can develop, either as a result of changes in the geostrophic circulation of the ocean or through atmospheric forcing, and a larger influence on the convective stability of the atmosphere should result. To quantify this statement, we compute the SST change δT required to produce a change in surface entropy equal to a given fraction F of the long-term winter mean $s_{tp} - s_o$ (denoted with an overbar):

$$\delta T = F(\overline{s_{tp} - s_o}) / \left(\frac{\partial s_o}{\partial T} \right)_{(\overline{T_s}, \overline{P_s})}. \quad (4)$$

In this expression, the sensitivity $(\partial s_o / \partial T)$ is evaluated at the long-term winter mean surface temperature ($\overline{T_s}$) and pressure ($\overline{P_s}$). The result is displayed in Figure 10 for a choice $F = 0.5$ (i.e. a 50% modulation of the mean tropopause to surface entropy difference). It is seen that over the Gulf Stream and the Kuroshio the SST changes required to impact significantly on atmospheric stability are modest (of the order of 1 K). Further analysis of the terms in (4) indicates that this arises because of low $\overline{s_{tp}} - \overline{s_o}$ and also because of the relatively large sensitivity $(\partial s_o / \partial T)$ found over these regions (not shown). Low SST changes are also required in the subtropical Atlantic; however, the latter region is an area of subsidence and therefore not relevant to the deep (surface-to-tropopause) convective mechanism studied here. Larger

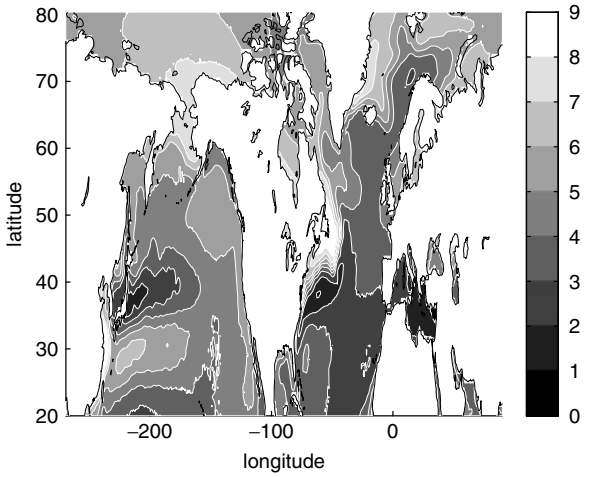

Figure 10. The SST change (contoured every K) required to match a 50% change in the entropy difference between the surface and tropopause in the Northern Hemisphere winter.

SST changes would be required elsewhere in the North Pacific and over the Labrador Current in the North Atlantic.

To make clear that low-frequency changes in SST are likely to have an impact on the convective stability of the atmosphere, we have estimated in Figure 11 the fraction F by which the mean wintertime tropopause to sea-surface entropy difference is modulated when setting δT in (4) to 80% of the amplitude of the observed decadal SST variability. The decadal SST was created by compositing the 10 yr smoothed SST records from the World Ocean Atlas (Locarnini *et al.*, 2010), Global Ocean Surface Temperature Atlas (Parker *et al.*, 1995), Kaplan (Kaplan *et al.*, 1998) and the NOAA extended reconstructed SST datasets (Smith *et al.*, 2008).

Consistent with the sensitivities shown in Figure 10, the resulting map shows that F can reach up to 40% in the Gulf Stream and Kuroshio (see Figure 11). This suggests that the ocean is highly capable of significantly modulating

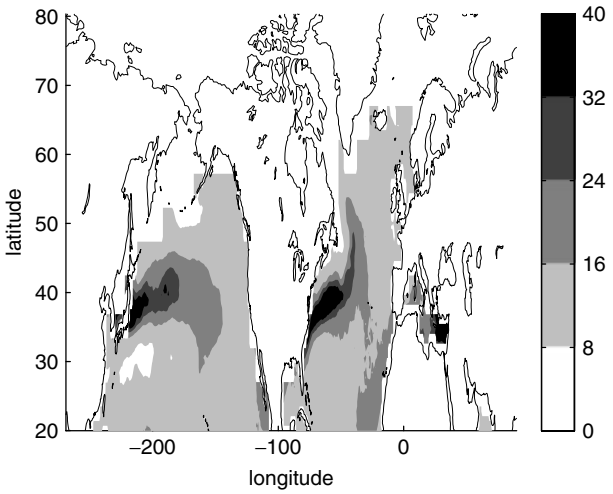

Figure 11. The fraction (F), in %, by which decadal SST variability can reduce the climatological wintertime entropy difference between the surface and the tropopause. See text for details of the calculation.

atmospheric stability in the extratropics on time-scales of decades and longer.

6. Conclusion

The main findings of our study can be summarized as follows:

- The western boundary currents are the oceanic regions where the extratropical atmosphere most likely convects in winter in both Southern and Northern Hemispheres. In summer, most of the convective activity over the oceans shifts equatorward of the western boundary currents, although it can still be detected over the Gulf Stream and the East Australian Current.
- The number of days per winter where the atmosphere is likely unstable to convection over a deep (surface-to-tropopause) layer shows great (30%) interannual variation over the midlatitude oceans. The source of this variation is, to first order, the erratic displacements of the storm tracks over ocean basins dictating, on any given day, where the tropopause is lower than on average.
- On intraseasonal time-scales the interaction of low-pressure systems with the ocean is self-limited by the generation of a cold SST anomaly over the western boundary currents. This negative feedback is weak because only a small SST anomaly (< 1 K) can develop in a few months. On interannual and longer time-scales, convective activity over the western boundary currents is likely to be strongly affected by changes in the ocean circulation.

These results are only diagnostic in that, although they suggest that western boundary currents are instrumental in setting when and where the atmosphere is most likely to convect in midlatitudes, they do not isolate the effect of these local air–sea interactions on the storm track, wind field, etc., over their respective ocean basins. It is hoped that the next generation of climate models will help in addressing this exciting question.

Acknowledgements

L. Sheldon is funded by both the Grantham Institute for Climate Change and the UK Met Office. Discussions with Cyril Morcrette helped in focusing the ideas presented in this article. Constructive comments from anonymous reviewers helped to improve the manuscript.

References

Berrisford P, Dee D, Fielding K, Fuentes M, Kallberg P, Kobayashi S, Uppala S. 2009. '*The ERA Interim Archive*', *ERA Report* Series 1, Technical Report. European Centre for Medium-Range Weather Forecasts: Reading, UK.

Chelton DB, Schlax MG, Freilich MH, Milliff RF. 2004. Satellite measurements reveal persistent small-scale features in ocean winds. *Science* **303**: 978–983.

Czaja A, Blunt N. 2011. A new mechanism for ocean–atmosphere coupling in mid-latitudes. *Q. J. R. Meteorol. Soc.* **137**: 1095–1101.

Czaja A, Frankignoul C. 2002. Observed impact of Atlantic SST anomalies on the North Atlantic Oscillation. *J. Climate* **15**: 606–623.

Emanuel KA. 1994. *Atmospheric Convection*. Oxford Univ. Press: Oxford, UK.

Frankignoul C. 1985. Sea surface temperature anomalies, planetary waves, and air–sea feedback in the middle latitudes. *Rev. Geophys.* **23**: 357–390.

Frankignoul C, Sennechael N, Kwon Y, Alexander M. 2011. Influence of the meridional shifts of the Kuroshio and the Oyashio extensions on the atmospheric circulation. *J. Climate* **24**: 762–777.

Hoskins BJ, McIntyre ME, Robertson AW. 1985. On the use and significance of isentropic potential vorticity maps. *Q. J. R. Meteorol. Soc.* **111**: 877–946.

Kaplan A, Cane M, Kushnir Y, Clement A, Blumenthal M, Rajagopalan B. 1998. Analyses of global sea-surface temperature 1856–1991. *J. Geophys. Res.* **103**: 18567–18589.

Kushnir Y, Robinson WA, Blade I, Hall NM, Peng S, Sutton R. 2002. Atmospheric GCM response to extratropical SST anomalies: Synthesis and evaluation. *J. Climate* **15**: 2233–2256.

Linkin ME, Nigam S. 2008. The North-Pacific Oscillation–West Pacific teleconnection pattern: Mature-phase structure and winter impacts. *J. Climate* **21**: 1979–1997.

Liu WT, Xie X, Niiler P. 2007. Ocean–atmosphere interaction over Agulhas extension meanders. *J. Climate* **20**: 5784–5798.

Locarnini RA, Mishonov AV, Antonov JI, Boyer TP, Garcia HE, Baranova OK, Zweng MM, Johnson DR. 2010. '*World Ocean Atlas 2009, Volume 1: Temperature*', Levitus S (ed.), NOAA Atlas. US Government Printing Office: Washington DC.

Minobe S, Kuwano-Yoshida A, Komori N, Xie S, Small RJ. 2008. Influence of the Gulf Stream on the troposphere. *Nature* **452**: 206–209.

Parker DE, Folland CK, Jackson M. 1995. Marine surface temperature: Observed variations and data requirements. *Climatic Change* **31**: 559–600.

Simmons AJ, Hoskins BJ, 1980. Barotropic influences on the growth and decay of nonlinear baroclinic waves. *J. Atmos. Sci.* **37**: 1679–1684.

Small R, DeSzoeke S, Xie S, O'Neill L, Seo H, Song Q, Cornillon P, Spall M, Minobe S. 2008. Air–sea interaction over ocean fronts and eddies. *Dyn. Atmos. Oceans* **45**: 274–319. DOI: 10.1016/j.dynatmoce.2008.01.001.

Smith TM, Reynolds RW, Peterson JC, Lawrimore J. 2008. Improvements to NOAA's historical merged land–ocean surface temperature analysis (1880–2006). *J. Climate* **21**: 2283–2296.

Tokinaga H, Tanimoto Y, Xie SP, Sampe T, Tomita H, Ichikawa H. 2009. Ocean frontal effects on the vertical development of clouds over the Western North Pacific: In situ and satellite observations. *J. Climate* **22**: 4241–4260.

Zhai X, Sheldon L. 2012. On the North Atlantic ocean heat content change between 1955–1970 and 1980–1995. *J. Climate.* **25**: 3619–3628.

